

Light-adapted charge-separated state of photosystem II: structural and functional dynamics of the closed reaction center

Gábor Sipka ¹, Melinda Magyar ¹, Alberto Mezzetti ^{2,3,†}, Parveen Akhtar ^{1,4}, Qingjun Zhu,⁵
 Yanan Xiao ⁵, Guangye Han ⁵, Stefano Santabarbara ^{6,†}, Jian-Ren Shen ^{5,7,†},
 Petar H. Lambrev ^{1,*†} and Gyöző Garab ^{1,8,*†}

- 1 Institute of Plant Biology, Biological Research Centre, Szeged, Hungary
- 2 Université Paris-Saclay, CEA, CNRS, Institute for Integrative Biology of the Cell (I2BC) 91191 Gif-sur-Yvette, France
- 3 Laboratoire de Réactivité de Surface UMR 7197, Sorbonne University, Paris, France
- 4 ELI-ALPS, ELI-HU Nonprofit Ltd., Szeged, Hungary
- 5 Photosynthesis Research Center, Key Laboratory of Photobiology, Institute of Botany, Chinese Academy of Sciences, Beijing, China
- 6 Photosynthetic Research Unit, Institute of Biophysics, National Research Council of Italy, Milano, Italy
- 7 Research Institute for Interdisciplinary Science, and Graduate School of Natural Science and Technology, Okayama University, Okayama, Japan
- 8 Faculty of Science, University of Ostrava, Ostrava, Czech Republic

*Author for correspondence: garab.gyozo@brc.hu (G.G.), lambrev.petar@brc.hu (P.H.L.).

†Senior authors.

G.G. conceived the study together with G.S., M.M., J.-R.S., and P.H.L. The Chl-*a* fluorescence and the flash-induced absorption kinetic devices were modified/constructed by G.S., and the measurements were performed and analyzed by G.S. and M.M. The low-temperature fluorescence emission spectroscopy measurements were carried out and analyzed by G.S. and S.S. The time-resolved fluorescence spectroscopy experiments were configured by P.H.L., G.S., and P.A. who also carried out the measurements and performed the model calculations; the electric field calculations were carried out by G.S. The rapid-scan FTIR spectroscopy measurements were performed and analyzed by M.M. and A.M. Whole cells and isolated PSII CC of *T. vulcanus* were provided by J.-R.S., Q.Z., Y.X., and G.H. The paper was written by G.G., G.S., M.M., P.H.L., P.A., S.S., A.M., and J.-R.S.

The authors responsible for distribution of materials integral to the findings presented in this article in accordance with the policy described in the Instructions for Authors (<https://academic.oup.com/plcell>) are: Gyöző Garab (garab.gyozo@brc.hu) and Petar H. Lambrev (lambrev.petar@brc.hu).

Abstract

Photosystem II (PSII) uses solar energy to oxidize water and delivers electrons for life on Earth. The photochemical reaction center of PSII is known to possess two stationary states. In the *open state* (PSII_O), the absorption of a single photon triggers electron-transfer steps, which convert PSII into the charge-separated *closed state* (PSII_C). Here, by using steady-state and time-resolved spectroscopic techniques on *Spinacia oleracea* and *Thermosynechococcus vulcanus* preparations, we show that additional illumination gradually transforms PSII_C into a *light-adapted charge-separated state* (PSII_L). The PSII_C-to-PSII_L transition, observed at all temperatures between 80 and 308 K, is responsible for a large part of the variable chlorophyll-*a* fluorescence (F_v) and is associated with subtle, dark-reversible reorganizations in the core complexes, protein conformational changes at noncryogenic temperatures, and marked variations in the rates of photochemical and photophysical reactions. The build-up of PSII_L requires a series of light-induced events generating rapidly recombining primary radical pairs, spaced by sufficient waiting times between these events—pointing to the roles of local electric-field transients and dielectric relaxation processes. We show that the maximum fluorescence level, F_m , is associated with PSII_L rather than with PSII_C, and thus the F_v/F_m parameter cannot be equated with the quantum efficiency of PSII photochemistry. Our findings resolve the controversies and explain the peculiar features of chlorophyll-*a* fluorescence kinetics, a tool to monitor the functional activity and the structural-functional plasticity of PSII in different wild-types and mutant organisms and under stress conditions.

IN A NUTSHELL

Background: Photosystem II (PSII), which uses solar energy to oxidize water and supplies the reducing equivalents necessary to fix carbon dioxide, is the engine of life. Monitoring the activity of PSII *in vivo* or *in vitro*, upon dark-to-light transition, is routinely performed by recording the rise of fluorescence intensity from the minimum (F_o) to the maximum (F_m) levels. The variable chlorophyll-*a* fluorescence ($F_v = F_m - F_o$) follows a complex induction kinetics and carries information on the functioning of the photosynthetic machinery. This is arguably one of the most commonly used techniques in plant biology. The F_v/F_m parameter, according to the mainstream model is equated with the quantum efficiency of PSII. According to this model, F_o and F_m belong to the open (PSII_o) and closed (PSII_c) states of the reaction center, states which, respectively, are ready and incapable of utilizing the absorbed light for stable charge separation. Although chlorophyll-*a* fluorescence measurements have provided a wealth of information on the mechanisms of photosynthetic light-energy conversion, the mainstream model is not free of controversies. Hence, our understanding of the photochemical activity of PSII remained fragmentary.

Questions: Our goal was to clarify the origin of chlorophyll-*a* fluorescence in association with the functional and conformational states of PSII.

Findings: We resolve the controversies and explain the peculiar features of chlorophyll-*a* fluorescence induction kinetics and show that in addition to PSII_o and PSII_c, this photosystem is capable of assuming light-adapted charge-separated state, PSII_L. Formation of PSII_L, via light-induced subtle conformational changes, facilitates the stabilization of charge-separated state. PSII_L is characterized by distinct features in the energy landscape of trapping/detrapping of excitations in the core-antenna reaction-center complex. The PSII_c–PSII_L transition is responsible for a large part of F_v , which thus appears to reflect the structural dynamics of PSII. Hence, the F_v/F_m parameter cannot be equated with the quantum efficiency of PSII photochemistry. Variations of this parameter – e.g. in mutants or upon exposing the organisms to different stress conditions – may be explained by changes in the functional activity of PSII or may reflect the structural-functional plasticity of this photosystem. Our data suggest key roles of strong local stationary and transient electric fields and dielectric relaxation processes during the operation of PSII.

Next steps: Further details of the reorganizations associated with PSII_c–PSII_L transitions and the underlying physical mechanisms should be uncovered, and mechanisms of natural, genetic and stress-induced variations in F_v investigated and correlated with structural-functional changes in PSII.

Introduction

Photosystem II (PSII) is a multisubunit enzyme that catalyzes the oxidation of water and the reduction of plastoquinone (Nelson and Yocum, 2006). In the *open-state* PSII (PSII_o), electron transfer, upon the absorption of one photon, starts with the formation of the primary radical pair $P680^+ \text{Pheo}^-$, which is stabilized via the re-oxidation of Pheo^- by the first, stable quinone acceptor molecule, Q_A , leading to a charge-separated state $P680^+ Q_A^-$. (Here, P680 and Pheo, following the conventional notations, refer to the primary electron donor from which charge separation starts, irrespective of its molecular identity, and pheophytin- a_{D1} , respectively.) In consecutive steps, $P680^+$ is re-reduced by the redox-active tyrosine (Y_Z), which then oxidizes the Mn_4CaO_5 cluster, producing the S_2 state of the oxygen-evolving complex (OEC). This generates a *closed-state* of PSII (PSII_c) with Q_A reduced. In this state, the light energy absorbed can produce only a rapidly recombining species, the $P680^+ \text{Pheo}^-$ radical pair (Sipka et al., 2019). PSII_c persists for several hundred microseconds, until the electron is transferred from Q_A^- to Q_B , the secondary quinone acceptor (Shlyk-Kerner et al., 2006). When this step is blocked by PSII inhibitor molecules, such as 3-(3',4'-dichlorophenyl)-1,1'-dimethylurea (DCMU), its lifetime becomes considerably longer, and PSII may assume a stationary state since the charge recombination between Q_A^- and $S_2^{(+)}$ is a thermally assisted de-trapping reaction (Tyystjarvi and Vass, 2004).

The activity of PSII is routinely tested using chlorophyll-*a* (Chl-*a*) fluorescence induction kinetics (Papageorgiou and Govindjee (2004) and references therein). To characterize the dark-to-light transition of PSII, either the *yield* or the *intensity* of the fluorescence emission is monitored. In both cases, the fluorescence levels rise from the minimum to the maximum, from F_o to F_m , or from O to P, respectively. The fast fluorescence transients usually contain intermediary states, J and I; these are absent when the electron transfer from Q_A^- to Q_B is inhibited, and then the O-to-P rise assumes a sigmoidal shape. According to the mainstream model, to reach F_m (or P) it is necessary, and sufficient, to have Q_A completely reduced in all the active PSII centers (Duysens and Sweers, 1963; Stirbet and Govindjee, 2012). Fluorescence lifetime measurements confirmed that the transition from F_o to F_m induced by the reduction of Q_A , upon continuous illumination, effectively corresponds to an increase in the lifetime (Holzwarth et al., 1985; Hodges and Moya, 1986; Roelofs et al., 1992) and, therefore, in the fluorescence yield resulting from center closure. In this framework, the F_v/F_m parameter represents an estimation of the maximal quantum efficiency of PSII ($F_v = F_m - F_o$; Butler, 1978; Duysens, 1978; Genty et al., 1989). The multiphasic (O–J–I–P) rise is explained by whole-chain electron-transfer reactions affecting the reduction state of Q_A (Strasser et al., 2004; Stirbet and Govindjee, 2012), and the sigmoidal rise is ascribed to an energetic coupling (connectivity) between PSII units (Joliot and Joliot, 1964; Lavergne and Trissl, 1995;

Stirbet, 2013). Despite the success of this widely used “ Q_A model”, it is not free of controversy (Joliot and Joliot, 1979; Vredenberg, 2011; Schansker et al., 2014; Magyar et al., 2018; Laisk and Oja, 2020). Also, in some cyanobacterial mutants (Vavilin et al., 1999) and wild-type green algal cells (Treves et al., 2016) no or very poor correlation is observed between the measured F_v/F_m parameter and the oxygen evolution activity of PSII.

The main problem with the Q_A model, i.e. that the redox state of Q_A accounts in full for the changes in fluorescence yield upon center closure, is that F_m cannot be reached upon reducing Q_A with a single-turnover saturating flash (STSF), and several additional flashes are required to complement F_v (Joliot and Joliot, 1979; Magyar et al., 2018). Also, to generate the O-to-P rise, multiple turnover saturating flashes (MTSFs) are required (Delosme, 1967; Schansker et al., 2011; Magyar et al., 2018). Recent investigations revealed the occurrence of conformational changes associated with F_v and uncovered the requirement of relatively long waiting times between the STSFs, hence the existence of rate-limiting steps that cannot be accounted for either by rapid photochemical reactions or by heterogeneity of PSII (Lavergne and Trissl, 1995) as discussed by Magyar et al. (2018). Evidently, after closing PSII, all STSFs (or surplus excitations) act on PSII_C. Hence, the gradual fluorescence rise, observed upon exposing PSII_C to a train of STSFs, strongly suggests the stepwise formation of a previously unidentified state of PSII—the *light-adapted charge-separated state* (PSII_L), which is characterized here at physiological and cryogenic temperatures. The PSII_C-to-PSII_L transition appears to be driven by transient, light-induced, electric fields but with rate-limiting processes, waiting times between effective excitations involved, which might be linked to dielectric relaxation. We show that PSII_L can be generated both in the monomeric and dimeric forms of PSII, demonstrating the occurrence of the sigmoidal rise of fast Chl-*a* fluorescence in the absence of connectivity between PSII units. Further, we provide irrevocable experimental evidence showing that the F_v/F_m parameter cannot be used to determine the quantum efficiency of PSII photochemistry. Our findings resolve the controversies regarding the origin of F_v and lay the foundations for a deeper understanding of the structural and functional changes during the dark-to-light transition of PSII in different organisms and mutants, as well as upon exposing plants to different stress conditions.

Results

Stepwise light-induced generation of PSII_L from PSII_C: Chl-*a* fluorescence transients

To investigate the possibility that in the dimeric PSII core complex (PSII CC) the charge-separated states of the two monomers influence each other, we compared the Chl-*a* fluorescence induction of DCMU-treated dimeric and monomeric PSII CC. The kinetics of the fast-fluorescence intensity transients of monomeric and dimeric complexes were virtually indistinguishable (Figure 1). Moreover, monomers,

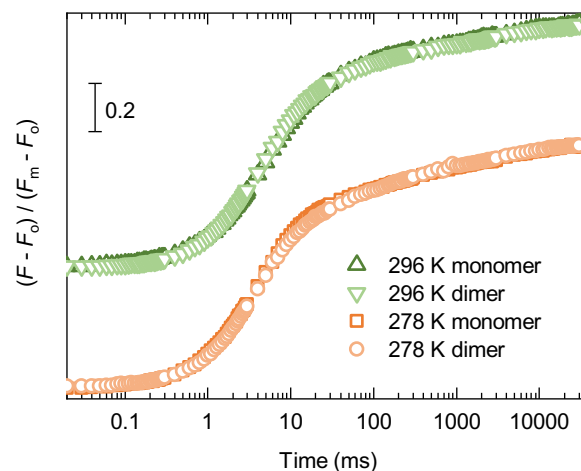


Figure 1 Fast Chl-*a* fluorescence rise of DCMU-treated solubilized monomeric and dimeric PSII core complexes of *T. vulcanus* at 278 and 296 K. The photon flux density of the excitation was 3500 $\mu\text{mol photons m}^{-2} \text{s}^{-1}$. (Note: curves at 296 K are upshifted for simpler comparison).

similarly to dimers, displayed a gradual rise of the fluorescence elicited by a train of STSFs (Supplemental Figure 1). These results indicate the absence of significant cooperativity between two monomers in the PSII CC of *Thermosynechococcus* (*T.*) *vulcanus*. Since the physiological state of PSII is a dimer (Shen, 1998), all further experiments using PSII CC were performed on its dimeric form.

To verify earlier conclusions that it is possible to increase the Chl-*a* fluorescence yield in the presence of reduced Q_A (PSII_C) and without inducing additional stable charge separation (Joliot and Joliot, 1979; Magyar et al., 2018; Sipka et al., 2019), we performed experiments on PSII CCs in which Q_A was pre-reduced with 2-mM dithionite. This treatment also prevented the formation of the S_2 state of the OEC, as evidenced by the absence of thermoluminescence (data not shown). (In the presence of DCMU alone, *T. vulcanus* PSII CC gives rise to the so-called Q-band due to $Q_A^-S_2^{(+)}$ recombination; Shen and Inoue, 1993.) Also, because of the prereduction of Q_A , the so-called C550 absorption band shift (Butler and Okayama, 1971) was not observed (Supplemental Figure 2). C550 is diagnostic of the presence of Q_A^- , via detecting the effect of local electric field on Pheo, an electrochromic band shift of the Q_x transition of Pheo_{D1} (Årsköld et al., 2003). As shown in Figure 2A, despite the pre-reduced Q_A , the train of STSFs was still capable of inducing fluorescence increments, gradually reaching F_m (PSII_L).

To avoid the possible involvement of alternative reductive electron-transfer pathways, we also recorded STSF-induced Chl-*a* fluorescence transients of DCMU-treated PSII CC in the presence of ferricyanide (FeCy; Figure 2B). Secondary electron transfer from cytochrome b_{559} (Cyt b_{559}) to P680⁺ (Tracewell and Brudvig 2008) and to tyrosine-D or the S_2 state of the OEC (Feyziyev et al., 2013) have earlier been shown to occur at cryogenic temperatures. Absorption

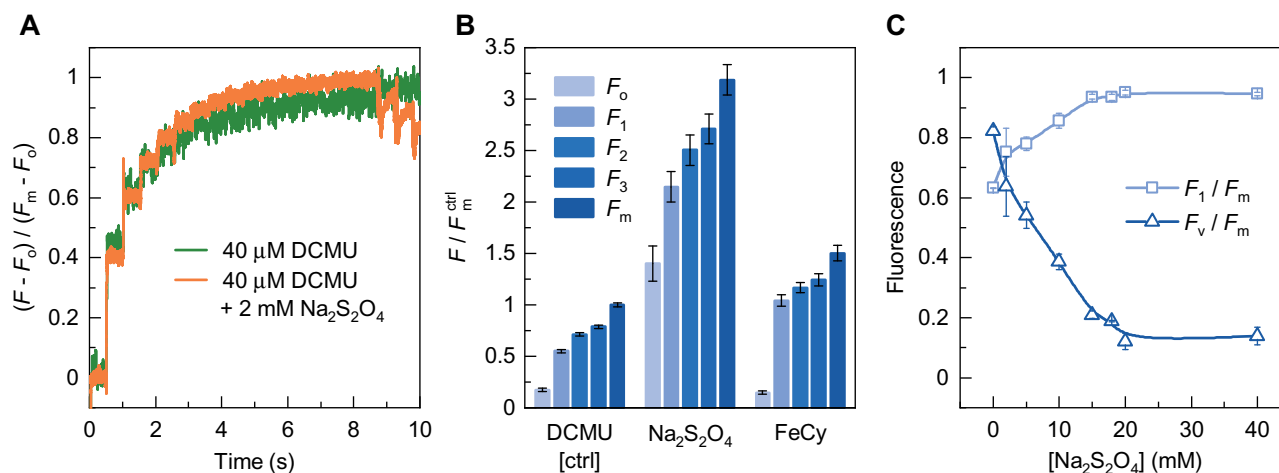


Figure 2 Effects of dithionite and FeCy on the variations of the STSF-induced Chl-*a* fluorescence yield of DCMU-treated PSII CC of *T. vulcanus* at 278 K. A, Kinetic traces, normalized to $F_m - F_0$, in the absence and presence of 2-mM dithionite, recorded with 1.6-kHz sampling rate; STSFs were applied 500 ms apart; at the end, three 200-ms long blue laser flashes were fired to ensure the saturation. B, Variations of the fluorescence yield parameters relative to the F_m level of the control (DCMU-treated PSII CC) in the absence and presence of 2-mM dithionite or 2-mM FeCy. F_1 , F_2 , and F_3 denote the levels after the first, second, and third STSF, respectively. C, Dependence of the F_1/F_m and F_v/F_m ratios on the concentration of dithionite.

transient measurements were carried out between 410 and 460 nm and 525 and 565 nm to estimate the significance of these reactions at room temperature. Our data show that electron donation from Cyt b_{559} occurs in <10% of the RCs, probably due to partial impairment of the donor side in some PSII CCs (Supplemental Figure 3). At the same time, FeCy exerted little effect on F_v . Similar to the DCMU-treated control (Magyar et al., 2018), the first STSF, which closed PSII, induced an $F_0 - F_1$ fluorescence rise ($F_1 < F_m$) but additional flashes were required to increase the fluorescence in a stepwise manner (producing $F_1 - F_2$, $F_2 - F_3$, etc. increments) before eventually, reaching F_m (Figure 2B).

Thus, it can be concluded that, albeit the overall fluorescence yields were affected by these treatments, the fluorescence increments were present in all cases. Very similar data were obtained at cryogenic temperatures and on isolated thylakoid membranes (Supplemental Figure 4—showing the STSF-induced Chl-*a* fluorescence transients of DCMU-treated thylakoid membranes at 213 K in the absence and presence of dithionite or FeCy). Hence, neither the prereluction of Q_A nor the oxidation of potentially active reducing components of PSII CC and the thylakoid membranes prevent the fluorescence increments. By using C550 and ΔA_{515} measurements on PSII CC of *T. vulcanus* and *Spinacia oleracea* thylakoid membranes, respectively, we confirmed the conclusion of (Joliot and Joliot, 1979) that the second STSF produced no additional stable charge separation (Supplemental Table 1), despite the fact that sufficiently long waiting times were allowed to induce the $F_1 - F_2$ increments.

The STSF-induced fluorescence increments could only be halted in the presence of high concentrations of dithionite (Figure 2C), which are known to pre-reduce Pheo (Klimov et al., 1977; Barber and Melis, 1990), and thus prevent the

formation of the $P680^+ \text{Pheo}^-$ radical pair. Hence, these data show that the flash-induced generation of the radical pair is a necessary condition to generate the fluorescence increments in PSII_C and thus to allow the light-induced formation of PSII_L. It is interesting to note that dithionite, while reducing (2 mM) or essentially eliminating (20 mM) F_v , also modulated the overall Chl-*a* fluorescence yield of PSII CC (Supplemental Table 2); at the same time, in spinach thylakoid membranes 2-mM dithionite exerted very little effect on F_{mv} , <10% increase compared to the control (Supplemental Figure 4C). (This difference between PSII CC and thylakoids might be due to different penetration ability of dithionite in the absence and presence of the bilayer lipid membrane.) These data strongly suggest that, similar to Chl-*a* (Connolly et al., 1982), the fluorescence yield depends on the physico-chemical environment of the emitter molecules.

Conformational changes and charge stabilization associated with the PSII_C–PSII_L transition: rapid-scan FTIR

Our earlier experiments have indicated the involvement of conformational changes associated with the fluorescence increments following the closure of PSII (Schansker et al., 2011; Magyar et al., 2018). To obtain information on the nature of these changes, rapid-scan Fourier transform infrared (FTIR) difference spectroscopy (Mezzetti and Leibl, 2017) experiments were performed on DCMU-treated PSII CC. Light-induced FTIR difference spectroscopy is a widely used technique to study the mechanism of photo-induced reactions in proteins, as it makes it possible to visualize changes not only in cofactors but also in the protein. Time-resolved FTIR difference spectra have the additional advantage of monitoring the kinetic evolution of these changes. Flash-induced time-resolved FTIR difference spectra were recorded

after exposing the sample to either 1 or 20 STSFs (Figure 3, A–C) and prominent changes in the 1,800–1,200 cm^{-1} region were observed. In this region, several marker bands have been identified in the past, such as the positive band at 1,478 cm^{-1} (semiquinone Q_A^- ; Berthomieu et al., 1990) or the negative band at 1,401 cm^{-1} (marker for the $S_1 \rightarrow S_2$ transition in the Mn cluster; Noguchi, 2007). Furthermore, in FTIR, difference spectra changes in the so-called amide I region (1690–1610 cm^{-1}) are indicative of conformational changes in the protein.

The double-difference spectra of the two transients revealed evident changes in the amide I region (Figure 3C). These data provide direct experimental evidence for the involvement of conformational changes associated with the F_1 – F_m fluorescence increment in the presence of DCMU. Earlier studies using time-resolved femtosecond serial X-ray crystallography have uncovered light-induced conformational changes at the Q_B –nonheme-iron region and the

OEC (Kern et al., 2013; Kupitz et al., 2014; Suga et al., 2017). These reactions are blocked in the presence of DCMU, and thus our data show that the structural dynamics of PSII is not confined to the OEC and the Q_B pocket.

Our measurements also revealed that at physiological temperature, 303 K, the relaxation of the FTIR signal after 20 STSFs was considerably slower than after one flash (cf. Figure 3, A and B), suggesting that the charge-separated state in PSII_L is more stable than in PSII_C. Indeed, the decay of both of the 1,401 cm^{-1} signal originating from the S_2 state of the OEC (Onoda et al., 2000), and the positive band 1,478 cm^{-1} , characteristic of Q_A^- were slowed down by about a factor of three in PSII_L compared to PSII_C (cf. Figure 3D). This conclusion is very similar to that obtained under comparable conditions on the stability of charge-separated state in purple bacterial reaction centers (bRCs; Malferrari et al., 2013). It should be emphasized that the fact that the OEC signal at 1,401 cm^{-1} decays with the

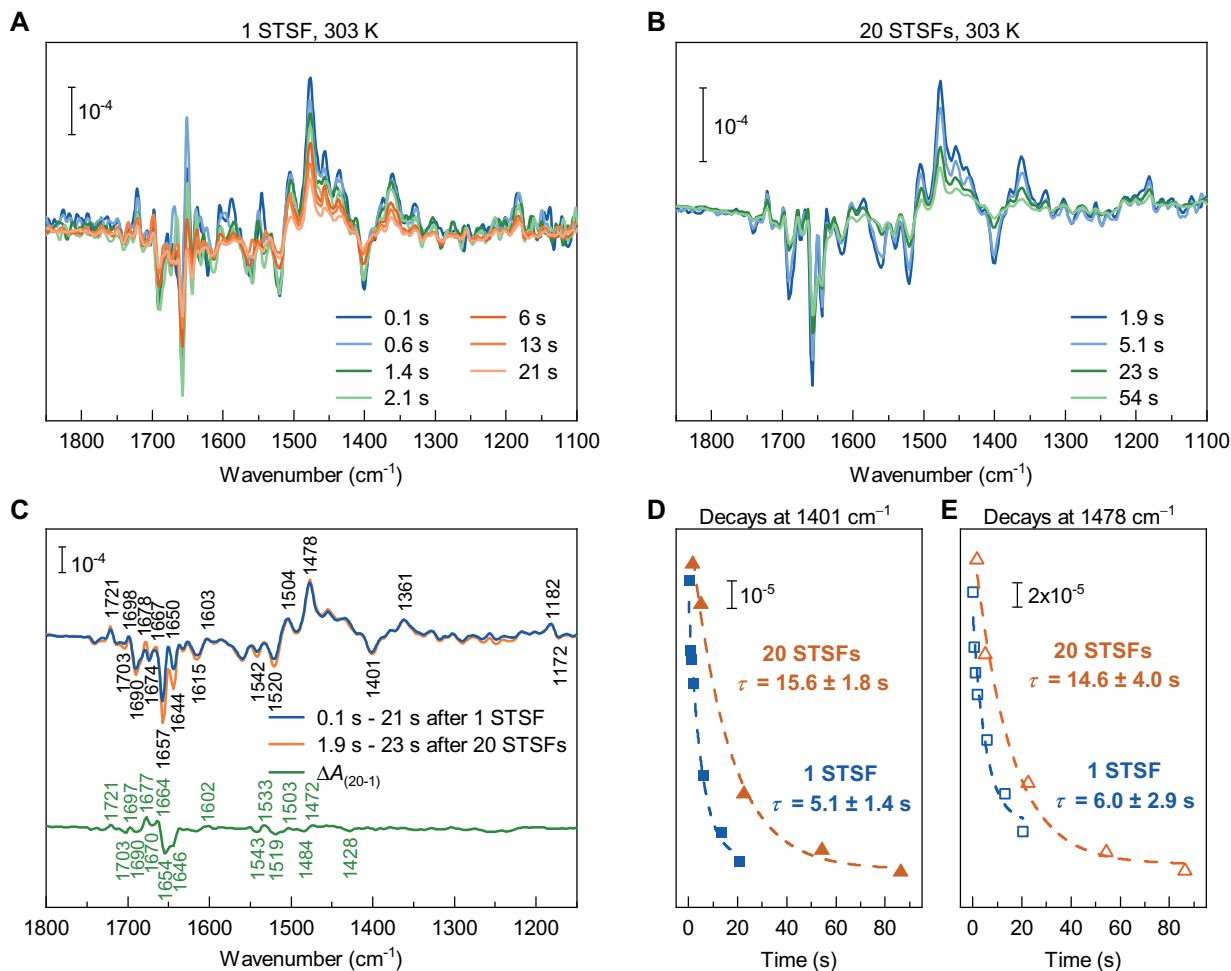


Figure 3 Time-resolved rapid-scan FTIR difference spectra and relaxation kinetics following 1 or 20 STSFs (saturating intensity 20 mJ), 532 nm, 7-ns laser flash) excitation of DCMU-treated PSII core particles at 303 K. Spectra recorded at different times, as indicated after one (A) or 20 (B) flash(es). C, Spectra of transients induced by 1 or 20 STSFs averaged as indicated by the label in the figure; and normalized to the band pair at 1,364/1,401 cm^{-1} , characteristic of the OEC (upper trace); and the PSII_L–PSII_C double-difference spectra (lower trace). D, Relaxation kinetics of the FTIR signal at 1,401 cm^{-1} , characteristic of the Mn cluster, and E, at 1,478 cm^{-1} , characteristic of the Q_A^- , after 1 and 20 flashes. The repetition rate of the train of laser flashes was 10 s^{-1} .

same kinetics of the Q_A^- signal at $1,478\text{ cm}^{-1}$ shows that in both cases (one flash and 20 STSFs) the predominant relaxation process is the $S_2Q_A^- \rightarrow S_1Q_A^-$ charge recombination.

Distribution of the excitation energy in PSII_O, PSII_C, and PSII_L: 80 K fluorescence emission spectroscopy

Low-temperature (80 K) fluorescence emission spectroscopy experiments were performed to characterize the distribution of excitation energy in PSII CC in the open, closed, and light-adapted charge-separated states. At and near liquid N₂ temperatures PSII CC has been shown to exhibit two main emission bands, at around 685 and 695 nm, originating from red-shifted Chl-*a* molecules located in the inner antenna complexes CP43 and CP47, respectively (Andrizhiyevskaya et al., 2005). The spectral shape is determined by a set of rate constants and reaction routes, exciton relaxations and exciton transfers between the reaction center (RC) and the two antenna complexes as well as the processes between domains of the protein complexes (Shibata et al., 2013).

Figure 4A shows the spectral variations during the Chl-*a* fluorescence emission in PSII CC during the induction caused by a series of sub-saturating light pulses. As shown in Figure 4B, the emission spectra of PSII_O and PSII_L—corresponding to F_o (approximately) and F_m —display considerably different shapes, wherein the ratio F_{685}/F_{695} significantly increased. Accordingly, the F_v/F_m spectrum exhibited a peak around 685 nm (Figure 4C). These changes cannot be assigned solely to the reduction of Q_A . The F_o – F_1 transition hardly affected the spectral distribution (Figure 4D) and the fluorescence yield, which increased by only about 10% compared to F_m . As shown in Supplemental Figure 5A, STSFs at 80 K were capable of generating sizeable fluorescence increase but the increments were much smaller than at higher temperatures, and F_m was not reached even after 500 flashes. This can be explained by the increased rigidity of the protein matrix of PSII CC at low temperature. This notion is supported by the data in Supplemental Figure 5B, showing that while at 233 K 20 STSFs nearly saturated F_v , at 173 K the same train of flashes generated a fluorescence yield which was only about 60% of F_m .

The above data clearly indicate that the most significant changes in the excitation energy distribution (irrespective of the underlying processes which determine the exact spectral profile of the fluorescence emission at 80 K) occur during the PSII_C–PSII_L transition, rather than upon the PSII_O–PSII_C step. Remarkably, PSII_L relaxes even at 80 K (Supplemental Figure 6), in accordance with our earlier observation on an intact leaf at 77 K (Magyar et al., 2018). The results are fully consistent with our earlier findings that, at cryogenic temperatures, only a small fraction of F_v arises from the closure of PSII (see also F_v with pre-reduced Q_A). It is also important to point out that the spectral variations reflect reorganizations, which affect the rates of energy or electron transfer (Shibata et al., 2013) in the PSII_L state. At cryogenic temperatures, equilibration with the low-energy Chls at CP47, responsible for the emission at 695 nm is

incomplete. Under these partial equilibration conditions, the RC can trap excitations from CP43 more effectively than from CP47. Consequently, if excitation trapping by the RC is slower from CP47, the F_{685}/F_{695} nm ratio is expected to increase. It is an interesting observation, in line with the involvement of conformational changes, that PSII CC appears to possess “memory” regarding its pre-illumination history at higher, but still cryogenic temperatures, where no relaxation of Q_A^- occurs. As shown in Supplemental Figure 7, the F_{685}/F_{695} ratio of the F_m spectra at 80 K can be enhanced by exposing the sample to a pre-illumination period at 233 K. This effect is reminiscent of the so-called Kleinfeld effect in bRC (Kleinfeld et al., 1984). It is equally interesting that the spectral distributions of the F_m states at 80 and 90 K resemble those in the F_o states at 90 and 100 K, respectively (Supplemental Figure 8), suggesting a complex energetic landscape linked to energy migration barriers that are very sensitive to the bath temperature, pointing also toward a possible role for local heat effects due to thermal dissipation (Cseh et al., 2000).

Changes in excitation kinetics upon PSII_C–PSII_L transition: time-resolved fluorescence spectroscopy

As shown above, the transition from PSII_C to PSII_L causes larger changes in the Chl-*a* fluorescence yield and emission spectrum than Q_A reduction does. To further examine the possible origin of the fluorescence changes, we measured the picosecond fluorescence decay kinetics of PSII CC in dark-adapted open state (F_o), dark-adapted closed state (F_1), and light-adapted state (F_m). At room temperature, we obtained essentially identical kinetics in F_o and F_m conditions as previously published by different groups (Szczepaniak et al., 2009; Caffari et al., 2011; van der Weijde Wit et al., 2011; Supplemental Figure 9). In F_o condition, the decay could be described by two main lifetimes of ~ 40 and 200 ps and an average fluorescence lifetime of 110 ps, whereas in F_m conditions decay lifetimes from 100 ps to 4 ns were resolved and the average lifetime increased to ~ 0.9 ns. To record the decay kinetics of PSII_C (F_1), STSFs were applied shortly before the excitation pulses eliciting the fluorescence emission—in practice the pre-illumination was done just outside the sample chamber ~ 4 s before the circulated sample solution reaches the measuring beam. To minimize the reoxidation of Q_A , the experiments were performed at 278 K in the presence of DCMU. Control F_o and F_m measurements were done under the same conditions but without the STSFs (F_o) or with additional preillumination (F_m). Despite the presence of a fraction of reopened RCs (resulting in a shorter average lifetime at F_m), the results showed that the sample was close to the ‘real’ F_o and F_m states (Figure 5) with an F_v/F_m ratio of 0.75 calculated from the average fluorescence lifetimes. While the fluorescence decay was much slower in F_m , the F_1 kinetics appeared to be closer to F_o than F_m (Figure 5A), confirming that the F_1 – F_m fluorescence increment is associated with changes in the excited-state lifetime of Chl. The kinetics at F_o and F_1 could

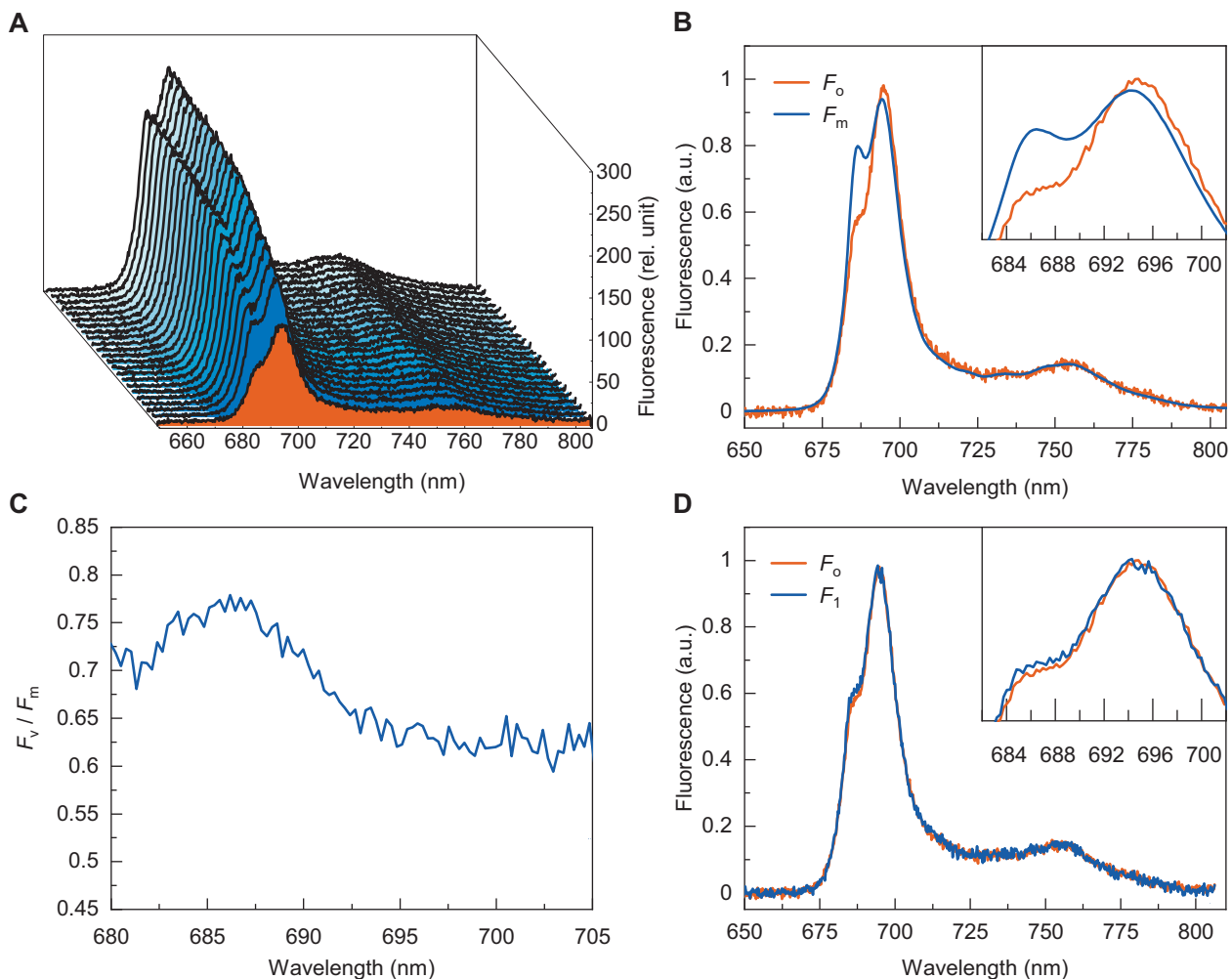


Figure 4 Spectral variations associated with F_v of DCMU-treated PSII CC *T. vulcanus* at 80 K—comparison of F_0 , F_1 and F_m . A, Fluorescence emission spectra measured in response to a train of 450 nm sub-saturating flashes from a pulsed LED recorded during Chl-*a* fluorescence induction at 80 K; the first spectrum (orange) represents the F_0 and the last one represents the F_m condition. B, Area-normalized fluorescence spectra—corresponding to F_0 and F_m states. C, The spectral distribution of the calculated F_v/F_m ratio. D, Area-normalized fluorescence emission spectra before and after pre-illumination with a STSF, corresponding to F_0 and F_1 , respectively. Shaded areas represent the SD of the measurements.

be described with a similar set of exponential decay lifetimes but the relative contribution of slower decay components (600 ps and 1.7 ns) increased in F_1 , so that the average lifetime increased from 110–160 to 220–360 ps, depending on the exact excitation conditions. In the F_m (PSII_L) state, displaying an average lifetime of 570 ps, all decay lifetimes were longer than in F_1 and the relative amplitudes of long-lived components grew further (Figure 5B).

The data confirm that the changes in the fluorescence yield upon converting PSII_C to PSII_L are caused by altered Chl-*a* excitation decay kinetics and indicate the presence of an efficient de-excitation channel in PSII_C other than the reduction of Q_A . The most likely mechanism of de-excitation in F_1 is nonradiative recombination of transiently generated radical pairs.

Currently there are several models for the excitation migration and trapping dynamics in PSII that fit the experimental data (van Amerongen and Croce, 2013). Irrespective

of the specifics of the kinetic model, if one considers dynamic equilibration between antenna exciton states and charge-separated states, then the overall excitation decay, and hence the fluorescence yield, depends on the electron-transfer reactions in the RC—the conventional explanation for the variable fluorescence. To gain further insight into the process, we modeled the F_1 and F_m fluorescence decays with a kinetic scheme comprising a sequence of four reversible steps (Figure 5). Global analysis of the spectrally resolved fluorescence kinetics showed that all lifetime components have virtually the same spectral shapes, indicating that the emission is from the same equilibrated pool of antenna pigments (Supplemental Figure 9). We further assume that the resolved decay lifetimes (50 ps and longer) are due to RC dynamics. Hence, only the first state (AntRC*), representing excited states, is emissive, whereas the following steps represent non-fluorescent charge-separated states (radical pairs RP_{1–3}). In such case, all rate constants (forward and

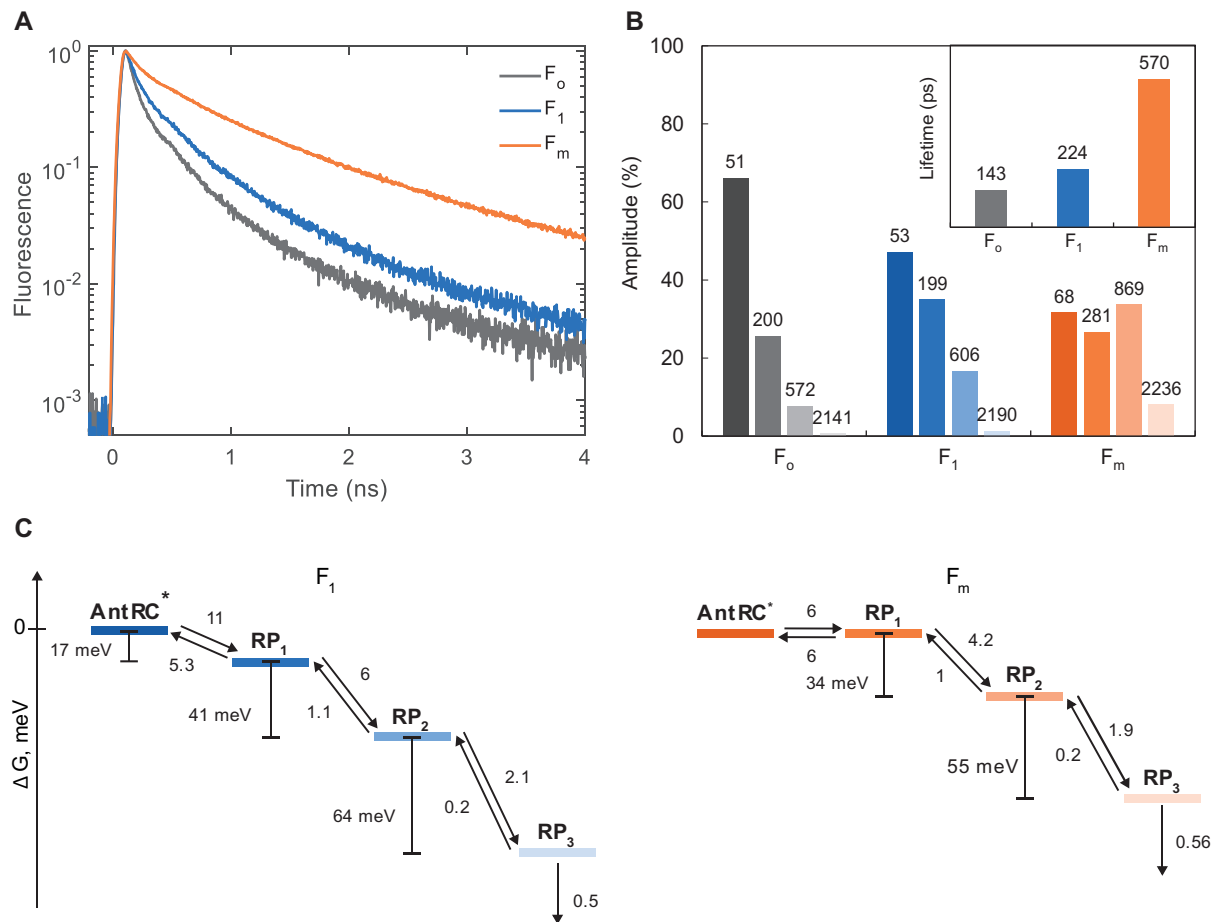


Figure 5 Fluorescence decay kinetics of DCMU-treated PSII CC of *T. vulcanus* under F_0 , F_1 , and F_m conditions. A, Fluorescence decays recorded at 278 K at 685 nm, excited at 632 nm. The slower decay under F_m conditions corresponds to the higher fluorescence yield. When the RCs are closed by a STSF, the decay (F_1) is only slightly slower compared to F_0 . B, Distribution of fluorescence lifetime components by their relative amplitudes (the lifetimes, in ps, are indicated above the bars). Inset: average fluorescence lifetimes. C, Gibbs free energy differences (ΔG) between different compartments of kinetic models—with three radical pairs—found for PSII core complex in both *charge-separated* (F_1 , left) and *light-adapted charge-separated* (F_m , right) state (all rates are given in ns^{-1}).

backward) can be independently determined by fitting the calculated time-dependent population of AntRC* to the fluorescence decay kinetics. The models fit the experimental data (Supplemental Figure 10) with residuals and χ^2 statistics equal to a free four-exponential fit (which has the same number of free parameters). The errors of the rate constants were estimated from the diagonal elements of the covariance matrix of the fit parameters as $\sigma_i = \sqrt{c_{ii}}$ and found to be within 3%–9%.

Antenna fluctuations could contribute to the kinetics on shorter timescales (Chmeliov et al., 2014) and, as pointed out above, the conditions to some extent deviate from the “true” F_1 and F_m ; therefore, we emphasize on the trend rather than the exact parameter values. Further, there can be different interpretations regarding the nature of the radical pair states, including different oxidation-reduction states of the RC cofactors as well as protein structural dynamics on a picosecond–nanosecond timescale (Szczepaniak et al.,

2009; Chmeliov et al., 2014). Regardless of the assignment, we observe that the forward reactions are slowed down in F_m compared to F_1 , shifting the equilibrium to the antenna exciton states and increasing the fluorescence lifetime and yield (Figure 5C). Thus, the time-resolved fluorescence data are in full agreement with the change in the steady-state fluorescence emission spectra upon F_1 – F_m transition. Correspondingly, the free energy gaps between all reaction intermediates are smaller in F_m than in F_1 . Since Q_A is reduced in both states, we must assume that the differences in the kinetics are caused by the local reconfiguration of the protein environment. For example, displacement and reorientation of polar residues can shift the midpoint potentials of the RC redox factors, altering the Gibbs free energy of forward electron transfer as well as charge recombination reactions. Such rearrangements will also affect exciton states with charge-transfer character or mixed exciton–charge-transfer states, key players in the primary photochemistry of

PSII (Romero et al., 2017), whose energy is strongly polarity-sensitive.

Discussion

Main attributes of the light-adapted charge-separated state of PSII

Our results point to the existence of a newly identified state, PSII_L, distinct from the dark-adapted closed-state PSII_C. The PSII_C–PSII_L transition is characterized by two quite peculiar features. First, in contrast to the PSII_O–PSII_C transition, which is generated by a single-photon absorption, PSII_L can be attained only in a stepwise manner, via multiple excitations of the sample following the closure of PSII (Figures 1, 2, and 4, and Supplemental Figures 4 and 5; see also Joliot and Joliot, 1979; Magyar et al., 2018). It is important to stress that during PSII_C–PSII_L transition, no additional stable charge separation can occur and the transition is driven by a series of rapidly recombining P680⁺Pheo[−] radical pairs (Magyar et al., 2018; Sipka et al., 2019). The other unique feature of this transition is that a radical pair, when generated “too early”, remains ineffectual. In other terms, the generation of the P680⁺Pheo[−] radical pair is only a necessary but not sufficient condition for the F_1 – F_m (PSII_C–PSII_L) transition. The excitations promoting the transition must arrive with sufficiently long waiting times ($\Delta\tau$) with respect to each other. This rate limitation has been shown to depend strongly on the temperature, with $\Delta\tau$ values four to six orders of magnitude larger than the lifetime of the primary radical pair (Magyar et al., 2018; Sipka et al., 2019).

Compared to PSII_C, PSII_L possesses several distinctive attributes. Beside the higher fluorescence of PSII_L (F_m) compared to F_1 in PSII_C (Figures 1–2), which is paralleled by an increase in the fluorescence decay lifetimes (Figure 5), and therefore an increase in fluorescence yield, PSII_L and PSII_C display distinct 80 K emission spectra (Figure 4). The latter is an indication of a change in the energy landscape of trapping/detrapping of excitations in the core antenna. The imposed energetic bottlenecks are very sensitive to temperature, as shown by the changes in emission bandshape upon cooling at cryogenic temperature even in a narrow temperature range (e.g. 80–100 K). These observations point to reorganizations in the protein matrix in the vicinity of the RC. Further, as revealed by our rapid-scan FTIR spectroscopy data, at noncryogenic temperatures the protein conformational states are also different in the two charge-separated states (Figure 3). Although PSII_L can be induced at cryogenic temperatures, similar to PSII_C, only PSII_L retains its capability of relaxing—albeit very slowly at low temperatures (Figure 4). In general, PSII_C and PSII_L exhibit different temperature dependences (Magyar et al., 2018).

Physical mechanism

With regard to the underlying physical mechanism, in accordance with our earlier work (Magyar et al., 2018), we propose that dielectric relaxation processes play key roles in the PSII_C–PSII_L transitions. Dielectric relaxations in the protein

matrix of PSII CC evidently occur in response to the stationary and transient electric fields around Q_A[−] and the P680⁺Pheo[−] radical pair, respectively (Supplemental Figure 11). This mechanism, akin to solvent polarization, is very similar to that offered to explain the light-induced conformational changes in bRCs. Conformational changes in bRC, affecting the electron transfer kinetics, have been reported by different authors (Kleinfeld et al., 1984; Nabedryk et al., 1990; Kálmán and Maróti, 1997; Abgaryan et al., 1998; Nagy et al., 2008). In the bRC, the electric field generated by light-induced charge separation has been proposed to perturb the molecular order, via dielectric relaxation (Kleinfeld et al., 1984; Nabedryk et al., 1990). Our rapid-scan FTIR data strongly suggest that the structural dynamics of PSII closely resembles that of the bRC (Mezzetti et al., 2002; Mezzetti and Leibl, 2017), the ancestor of PSII (Cardona et al., 2012). The structural dynamics can also be related to the photoinduced volume contraction via electrostriction, observed both in the bRC and PSII CC (Hou et al., 2001).

Dielectric relaxation processes with a broad range of lifetimes, and different dominance at different temperature intervals have been shown to occur in hydrated proteins (Nakanishi and Sokolov, 2015). In the temperature range allowing motions in the protein moiety, the relaxation processes are manifested in changes that can be detected by time resolved FTIR measurements (Figure 3). At lower temperatures, other, slower relaxation processes may explain our observations. In general, electric fields have been shown to affect the functioning of enzymes (Fried and Boxer, 2017), and that of PSII in particular (Dau and Sauer, 1992; Vredenberg, 2011; Laisk and Oja, 2020), also at cryogenic temperatures (Knox et al., 1984). It is to be noted here that the stationary and transient local electric fields in the PSII RC are at least an order of magnitude stronger than the uniform transmembrane fields in thylakoid membranes (Zimányi and Garab, 1989)—generated during the operation of the vectorial electron transport (Laisk and Oja, 2020) or exposed by ion gradients (Witt, 1979; Dau and Sauer, 1992). A nonconflicting hypothesis is that local-heat effects (Cseh et al., 2000), due to dissipation accompanying the recombination of charges of the primary radical pair, facilitate the conformational transitions. Nevertheless, the explanation based on the physical mechanism of dielectric relaxation, with or without the local heat, must be complemented in order to satisfy the special conditions for the generation of the PSII_L state. In particular, there are rate limitations in Chl-*a* fluorescence, i.e. P680⁺Pheo[−] induces increments *only* if it is generated by a sufficiently long waiting time after the reduction of Q_A[−] or after the consecutive steps. The occurrence of waiting times suggests that slow relaxation processes in the protein matrix play an important role. Because of the rigidity of the protein matrix, the relaxation appears to be incomplete (leading only to the F_o – F_1 rise), and further excitations are required to gradually induce F_m . Such excitation can be achieved by generating the P680⁺Pheo[−] radical pairs. The sequence of putative events

following the reduction of Q_A is schematically illustrated in Figure 6.

The ns transient electric field of the primary radical pair strongly perturbs the local electric field around Q_A^- : on the Q_A side of the radical pair, the negative potential will be transiently increased by the presence of Pheo^- ; also, on the donor side, the weak positive potential, arising from S_2^+ , will be transiently “replaced” by a very strong positive potential due to P680^+ (for a schematic illustration, see Supplemental Figure 9). It is reasonable to assume that this nonequilibrium configuration of the dielectric matrix relaxes orders of magnitude slower than the transient field itself. One can also argue that this perturbation facilitates to complete the dielectric relaxation around Q_A^- . Elucidation of the molecular and physical mechanisms is beyond the scope of the present study. Nevertheless, in broad terms, the observed stabilization of the charge-separated state by multiple STSFs and the strong temperature dependence of the STSF-induced Chl-*a* fluorescence increments are in harmony with the mechanism outlined above.

Physiological role of the formation of PSII_L: Chl-*a* fluorescence transients

Photosystem II is the engine of life: by oxidizing water, it provides photosynthesis with an unlimited supply of reducing equivalents to reduce carbon dioxide to carbohydrates, which is the energetic basis of virtually all life on Earth (Barber, 2004). For these reasons, monitoring PSII activity is important in most plant physiology studies. Such investigations are routinely performed by measuring the Chl-*a* fluorescence induction, a noninvasive measuring technique that can be applied on leaves, algal, or cyanobacterial cells under

a variety of physiologically important experimental and environmental conditions, as well as on isolated thylakoids and PSII particles. Chl-*a* fluorescence is one of the most widely employed techniques in plant biology, and the F_v/F_m parameter is certainly the most used Chl fluorescence parameter in the world. The main purpose of measuring this parameter is to determine the maximum quantum efficiency of PSII photochemistry, which is typically attained in dark-adapted samples when the plastoquinone pool is fully oxidized.

The key assumptions behind equating the F_v/F_m ratio with the maximum quantum efficiency of PSII photochemistry are that at F_o PSII centers are maximally quenched by photochemistry (open centers) and at F_m the photochemical quenching is absent (closed centers; Stirbet and Govindjee, 2012). The latter condition is often equated to the Q_A being reduced. However, now irrevocable experimental evidence shows that the reduction of Q_A alone is not a sufficient requisite for attaining F_m . Clearly, F_m cannot be reached by a STSF, despite closing all PSII (Figure 2, see also Joliot and Joliot 1979; Magyar et al., 2018; Sipka et al., 2019; Laisk and Oja, 2020). Also, the corresponding F_v/F_m values of PSII_C, i.e. measured after the first STSF inducing stable charge separation in all active centers under physiologically relevant conditions, are typically not higher than 0.5 (Figure 2), and can be much lower at cryogenic temperatures (Figure 4). In contrast, the quantum efficiency of the stable charge separation in PSII is thought to be close to unity at all temperatures (Romero et al., 2017). Further, closing the RC by chemically pre-reducing Q_A does not prevent the light-induced Chl-*a* fluorescence transitions (Figure 2). For these reasons, the physical mechanism of F_v must be laid on new grounds, which beside the reduction of Q_A consider the

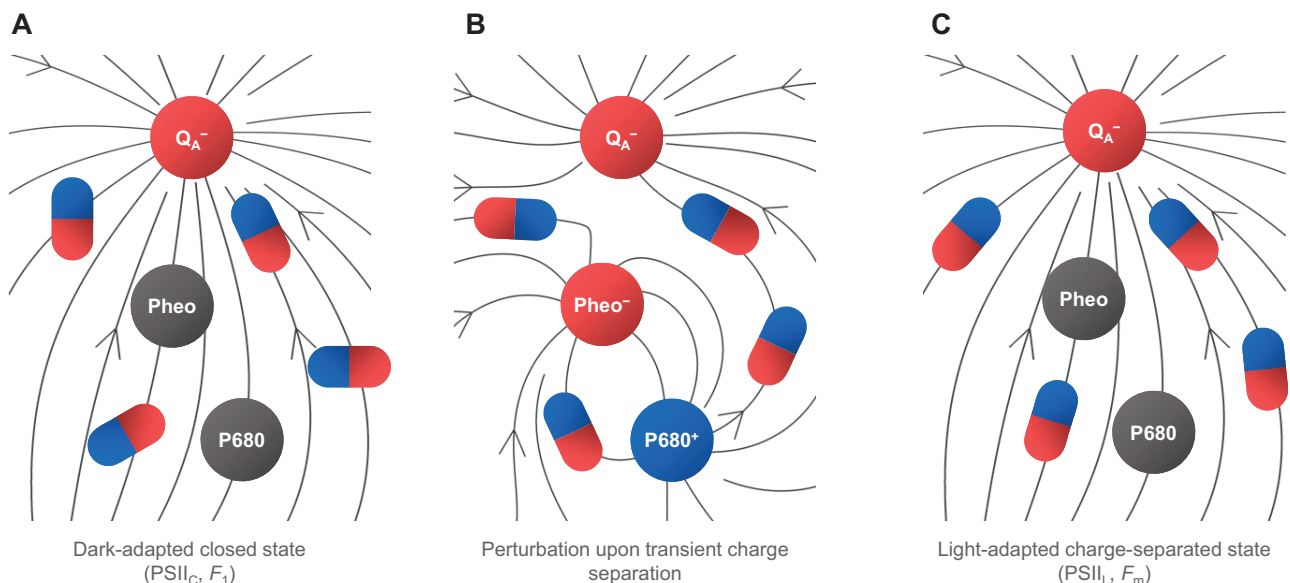


Figure 6 Schematic illustration of the behavior of the dielectric matrix in stationary and transient electric fields—leading to the formation of the PSII_L state. A, Charge-separated closed state of dark-adapted PSII, generated by a STSF; B, perturbation of the Q_A^- stationary field by a transient charge separation; C, fully relaxed charge-separated state (PSII_L) formed after several transient charge separation events. The circles represent the primary redox cofactors in the RC and the schematic dipoles illustrate the readjustment of the dielectric matrix to the local electric field, represented by the field vectors (arrowed lines). For the corresponding potential profiles, see Supplemental Figure 11.

reconfiguration of PSII to a functional state in which stable photochemistry is actually prevented. Thus, our data strongly suggest that the F_v/F_m parameter is determined, in large part, by the structural dynamics of PSII. The strong correlation between the photochemical efficiency of PSII and the magnitude of the F_v/F_m parameter observed using MTSFs and continuous wave irradiation (Genty et al., 1989; Papageorgiou and Govindjee, 2004) indicates that the structural dynamics are part of PSII functionality under physiological conditions. At the same time, estimation of both the maximal photochemical efficiency of PSII and, particularly, of the Q_A (or plastoquinone) redox level by STSFs would be biased. However, even this correlation cannot be taken for granted, as shown by reported cases in which efficient functioning of PSII is not accompanied by sizeable F_v (Vavilin et al., 1999; Treves et al., 2016). It remains to be investigated if the deficiency of F_v in these cases is due to the lack of structural dynamics upon the PSII_C–PSII_L transition, or, what seems more likely, due to a different organization of the pigment molecules or of the protein matrix. In general, testing the functional activity of PSII by using the F_v/F_m parameter requires a cautious approach and in special cases, e.g. under stress conditions or in mutants, independent investigations should be carried out to reveal the underlying physical mechanisms and the physiological status of PSII.

Another physiologically important attribute of oxygenic photosynthetic organisms is their capability of quenching the excess excitation energy, i.e. the fraction of absorbed light which cannot be utilized for photosynthesis, by a process called nonphotochemical quenching (NPQ) of the first singlet-excited state of Chl-*a*, aka NPQ of Chl-*a* fluorescence (Demmig-Adams et al., 2014; Ruban, 2016). To determine the magnitude and kinetics of NPQ, the most commonly used Chl-*a* fluorescence measuring and imaging techniques are based on generating the maximum fluorescence levels—using MTSFs—before, during, and after the actinic illumination. This is performed with the aim to close PSII and to account for the contribution of the photochemical quenching due to stable charge separation. However, since both MTSFs and the actinic illumination evidently lead to the formation of PSII_L, rather than merely generating and retaining PSII_C, contributions from factors other than processes in the antenna cannot be a priori ruled out. In fact, it has recently been shown that the magnitude of NPQ depends strongly on the state (F_o versus F_m) of PSII (Farooq et al., 2018).

Another parameter of physiological importance, which is frequently derived from the sigmoidal rise of fluorescence in the presence of DCMU, is the connectivity of PSII units (Joliot and Joliot, 1964; Stirbet, 2013). It is clear, however, that sigmoidal rises, observed on isolated monomeric and dimeric PSII CCs (Figure 1), originate from several successive photoreactions spaced by waiting times between consecutive excitations, as already pointed out by Magyar et al. (2018; see also Schansker et al., 2011; Vredenberg, 2011).

Last but not least, we would like to stress that Chl-*a* fluorescence transitions cannot be understood without taking

into account the rate-limiting steps in the fluorescence induction, i.e. the waiting times ($\Delta\tau$) between excitations that are required for the effectiveness of excitations to induce fluorescence increments after closing PSII (Magyar et al., 2018). This is a somewhat odd but crucial novel experimental observation by Magyar et al. (2018), which is nevertheless fully consistent with earlier observations (Joliot and Joliot, 1979; France et al., 1992). It must also be emphasized here that $\Delta\tau$ does not mean gating of the primary charge separation events, i.e. the generation of the $P680^+Pheo^-$ radical pair (Sipka et al., 2019). In fact, the fluorescence increments during the PSII_C–PSII_L transition appear to be driven by the rapidly recombining local electric-field transients due to these radical pairs—but only if they are generated with a sufficiently long waiting time. Qualitatively, the $\Delta\tau$ -dependent fluorescence increments offer explanation on the peculiarity of the fast (O–J–I–P) Chl-*a* fluorescence induction kinetics of PSII in the absence of PSII inhibitor and under physiologically relevant conditions. The conundrum concerning these transitions had been that only the initial (O–J) step of these transitions, the so-called photochemical phase, could be ascribed to photochemistry (Delosme, 1967), and the nature of the remaining (J–I–P) phases, originally termed thermal phase, had remained elusive. Some data suggested an origin in conformational changes (cf. Schansker et al., 2014 and references therein), while others linked it to the operation of the linear electron transport chain, and the reduction of the entire intersystem electron transport system (Stirbet and Govindjee, 2012). As already briefly outlined by Magyar et al. (2018), by using the condition of waiting time, we can at least qualitatively explain why the so-called photochemical, O–J phase in the O–J–I–P transient does not reach the P level even in extremely high light (Schansker et al., 2011). In this case, the rate-limited rise of the fluorescence emission competes with the re-oxidation of Q_A^- by Q_B (Shlyk-Kerner et al., 2006), which reopens PSII, and thus leads to a dip (J–I phase). The rise is then resumed in the I–P phase, upon the re-reduction of Q_A , and the reduction of the entire electron transport chain—in good accordance with the explanation by Stirbet and Govindjee (2012) as well as the finding that the I–P phase depends on the activity of photosystem I (Schansker et al., 2005; Ceppi et al., 2012).

In conclusion, here we have shown that in addition to the two well-known stationary states of functionally active PSII, the open and closed states, PSII_O and PSII_C, respectively, this photosystem can also assume light-adapted charge-separated state, PSII_L. Formation of this latter state is shown to facilitate stabilization of the charge-separated state. The PSII_C–PSII_L transition is associated with a large part of F_v , the variable Chl-*a* fluorescence, and appears to reflect the structural dynamics of PSII. These data cannot be reconciled with the most widely accepted model, the Q_A model, according to which F_v originates solely from the PSII_O-to-PSII_C transition. Accordingly, the F_v/F_m parameter should not be equated with the quantum efficiency of PSII

photochemistry while this parameter might still be used to monitor the functioning of PSII. Estimation of Q_A and the PQ redox pool by fluorescence-based methods might suffer from even larger interpretation biases and should therefore be adopted with caution to compare the activity of PSII on the same organism and under comparable conditions. Our data also show that the sigmoidal rise of the Chl-*a* fluorescence induction, in the presence of PSII inhibitor, should not be used to measure the connectivity of PSII units. By using the rate-limiting step in F_v identified earlier, and taking into account the “competing” event, the reopening of PSII upon the reoxidation of Q_A by Q_B , we offer a qualitative explanation of the fast (O–J–I–P) Chl-*a* fluorescence transient which, with its I–P transition in agreement with the generally accepted view within the frameworks of the Q_A model, depends on the functioning of the entire linear electron transport system. Regarding the physical mechanisms, our data strongly suggest that intense stationary and transient local electric fields and dielectric relaxation processes play key roles. Elucidation of the nature of the evidently subtle reorganizations and of the underlying physical mechanisms—especially during the waiting times—will most certainly provide further crucial information on the structural dynamics of PSII.

Materials and methods

Source material

Thermosynechococcus vulcanus, a thermophilic cyanobacterial strain isolated from a hot spring in Yunomine, Japan (Koike and Inoue, 1983), was grown as a batch culture. Spinach (*S. oleracea*) was purchased from a local growers' market.

Growth conditions

Thermosynechococcus vulcanus cells were grown in BG11 medium (pH 7) at 323 K under continuous illumination with a white fluorescent lamp at intensity of 50–100 $\mu\text{mol photons m}^{-2} \text{ s}^{-1}$ photon flux density (Shen et al., 2011). Cultures were aerated on a gyratory shaker operating at 120–150 r.p.m. to exponential growth phase.

Sample preparation

Thylakoid membranes were isolated from fresh spinach (*S. oleracea*) leaves essentially as described earlier (Chylla et al., 1987), with minor modifications. Briefly, deveined leaves were homogenized in a resuspension medium containing 50-mM tricine (pH 7.5), 400-mM sorbitol, 5-mM KCl, 2-mM MgCl_2 , filtered through a nylon mesh and the supernatant was centrifuged for 7 min at 6,000g. The pellet was resuspended in a hypotonic medium containing 50-mM Tricine (pH 7.5), 5-mM KCl, and 5-mM MgCl_2 , followed by the immediate addition of the resuspension medium supplemented with 800 mM Sorbitol before centrifugation for 7 min at 6,000g. The pellet was finally resuspended in the resuspension medium and stored in liquid nitrogen at a

concentration of 2–3 mg mL^{-1} Chl. Identical results were obtained with fresh preparations.

PSII core complexes of *T. vulcanus* were isolated as described earlier (Shen and Inoue, 1993; Shen and Kamiya, 2000; Kawakami and Shen, 2018). For all the experiments, the isolated PSII CCs were diluted in a reaction buffer medium containing 5% glycerol, 20-mM MES (pH 6.0), 20-mM NaCl, 3-mM CaCl_2 .

Fluorescence yield measurements

Relative fluorescence yields were measured using a PAM (Pulse Amplitude Modulation) 101 fluorometer (Walz, Effeltrich, Germany). The frequency of the modulated measuring light (low intensity, nonactinic) was 1.6 kHz. Variable fluorescence was induced by STSFs (Xe flashes, Excelitas LS-1130-3 Flashpac with FX-1163 Flashtube with reflector) of 1.5- μs duration at half-peak intensity. The sample was placed at the sample holder of a thermoluminescence apparatus in order to control the temperature. The timing of the flashes was controlled by using a home-designed programmable digital pulse generator. The decays of each measurement were recorded by using a National Instrument data acquisition device (DAQ 6001) via custom-designed LabVIEW software. Least-squares optimization was used to estimate the decay parameters. The optimization algorithms were implemented in Matlab (The MathWorks, Natick, MA, USA). For Chl-*a* fluorescence transient measurements the Chl concentration of the thylakoid membranes were diluted to $\sim 100 \mu\text{g mL}^{-1}$ in resuspension medium; the PSII CC to $\sim 25\text{--}50 \mu\text{g mL}^{-1}$ in reaction buffer. DCMU was dissolved in dimethyl sulfoxide (DMSO) and added to all samples immediately before the fluorescence measurements at a final concentration of 40 μM (the final concentration of DMSO did not exceed 1%). Before the measurements, the samples were dark adapted for 5 min at room temperature. In the case of dithionite, after 2 min of dark adaptation with the dithionite, DCMU was added, and the sample was dark adapted for 5 min before the measurement. In the case of FeCy, first DCMU was added to avoid the Ikegami-Katoh effect (Ikegami and Katoh, 1973), and after 5-min dark adaptation 2-mM FeCy was also added to the mixture.

FTIR measurements

For FTIR measurements, PSII CCs (corresponding to Chl concentrations between 2.5 and 4 mg mL^{-1} , depending on the batch used) were prepared as thin paste squeezed between two CaF_2 windows to yield an absorbance in the amide I region of the spectrum of 0.7–0.9 OD. The sample cell was sealed with silicone grease. To block the Q_A -to- Q_B electron transfer, DCMU was added to the PSII CC suspension. The sample was kept in a nitrogen cryostat (Oxford Instruments) to keep the temperature at 303 K stable during the measurements. The sample was stabilized in the dark for more than 2 h before the spectra were recorded.

Time-resolved rapid-scan FTIR difference spectra were recorded using a Bruker IFS88 FTIR spectrometer equipped with a photoconductive MCT-A (Mercury Cadmium

Telluride - narrow band) detector at 4 cm^{-1} resolution and OPUS software, following the approach of Mezzetti and co-workers (Mezzetti et al., 2002). Spectra were recorded in time windows of different durations (increasing with the time distance from the flash or from the 20 flashes sequence); this allowed recording the decay of the signal with a better signal-to-noise ratio (S/N). The photoreaction was triggered by one (or 20, fired at 10 Hz) saturating flash from a frequency-doubled Nd:YAG laser (Quantel) delivering 20-mJ pulses of 7-ns width. Synchronization between laser flashes and the recording of interferograms was checked on a digital oscilloscope. The temperature was set using a nitrogen flux Oxford Instrument cryostat.

The results from several cycles (obtained on at least three different samples) were averaged to improve the S/N ratio. At 303 K, an appropriate delay time between cycles (10 min and 20 min after 1 and 20 flashes, respectively) allowed a complete recovery of the RC neutral state after the light-induced charge separation.

Steady-state absorption spectroscopy

Absorption spectra, in the range of 350–750 nm, were recorded at room temperature with a Thermo Evolution 500 spectrophotometer. PSII CC samples in solution were diluted in reaction buffer to an absorbance of 1.0 at the red maximum. Measurements were performed in a semi-micro quartz cell of 1-cm optical path length.

Flash-induced absorption change measurements

The kinetic traces of absorption changes were detected by a home-constructed single-beam kinetic spectrophotometer according to (Büchel and Garab, 1995; Sipka et al., 2018). The kinetics of absorption changes were induced by STSFs (Xe flashes of Excelitas LS-1130-3 Flashpac with FX-1163 Flashtube with reflector) of 1.5- μs duration at half-peak intensity. The actinic flashes were passed through a Schott RG630 filter. For the measuring light, a Schott KL 2500 LED lamp was used. A monochromator (Bausch & Lomb with a concave holographic grating) was used to disperse the measuring light. The monochromatic, transmitted measuring light was detected by a photomultiplier (EMI 9558 B, protected by a Corning 4-96 filter) which was connected to a differential amplifier and to a digital oscilloscope (Analog Discovery 2 100-MSPS USB Oscilloscope). For the synchronization of the flash lamps during the measurements, the shutter and the oscilloscope were controlled by a programmable digital pulse generator (BNC 577, Berkeley Nucleonics Corp) via custom-designed LabVIEW software. To increase the S/N ratio, 8–128 kinetic traces were averaged depending on the required S/N. Samples were placed in a semi-micro quartz cuvette (of 10-mm optical pathlength and 2-mm width). The STSF-induced energization of the thylakoid membranes was monitored by the electrochromic band shift of the carotenoids at 515 nm. The electrochromic signal at a given wavelength was calculated from the kinetic traces at 2 ms after the flash. On PSII CC, flash-induced absorption changes were monitored between 410 and 460 nm and 515

and 565 nm. All measurements were carried out at room temperature. Thylakoid membranes were suspended in the resuspension medium; PSII CCs were suspended in the reaction buffer; in all cases, the samples were anaerobically dark adapted for 5 min prior to measurement.

Low-temperature fluorescence spectroscopy

Steady-state fluorescence emission spectra were recorded in the 80–300 K range on a high-sensitivity fluorescence set-up, taking into account the spectral/temporal variation of fluorescence yield due to photochemical trapping and other processes on nonphotochemical origin of isolated PSII CC. The laboratory-assembled fluorimeter was equipped with a shutter-protected liquid nitrogen cooled charge-coupled device (CCD) camera (Princeton Applied Research, LN/CCD-ST138), coupled to a spectrometer (SpectraPro-300i, Princeton; Nematov et al., 2017). An OG570 (Schott) band-pass filter was placed before the spectrograph to reduce scattered and stray excitation light. The fluorescence excitation source was a LED (LumiLeds LXML-PR02-1050), controlled by a laboratory-assembled driver/pulser, which allowed synchronization with the detection camera electronic control unit (Princeton Applied Research, ST138) that has its built-in triggering capability, as well as the synchronization of an additional pulsed light source (Xe-Flashlamp) for single-turnover flash (STF) excitation. The LED pulse-length, repetition rate, and intensity were also controlled by the laboratory-assembled pulser/driver. The LED pulse intensity was further attenuated by neutral density filters to approx. $0.14\text{-}\mu\text{mol photons s}^{-1}\text{ m}^{-2}$. Spectra were acquiring by setting the LED flash within the opening time of CCD-protecting shutter (software controlled, Roper Instrument, WinSpec32), whereas STFs were fired during the shutter dark time, and proved by successive LED pulses, Spectra collected close to F_o condition (Rizzo et al., 2014; Remelli and Santabarbara, 2018) was tested either with 1-, 2-, 5-, and 10-ms LED pulse duration; there was no difference in the spectra, but in the S/N. To obtain F_1 or F_o (approx.), the spectra were measured after the first LED pulse excitation with or without pre-STSF illumination, respectively; for STSF excitations an Excelitas LS-1130-3 Flashpac with FX-1163 Flashtube with reflector of 1.5- μs duration at half-peak intensity was used. For F_1 and F_o , only the first spectra of each measurement were averaged ($n = 8$). F_m was reached with multiple Xe-flash illuminations and/or continuous ($\sim 100\text{ s}$) LED excitation; on the plateau, about hundred spectra were averaged to obtain the F_m spectra. Spectra were acquired at a resolution of 0.25 nm per pixel and corrected for the wavelength sensitivity of the detector. Samples were diluted to a Chl-*a* concentration of $5\text{ }\mu\text{g mL}^{-1}$; DCMU was added at $40\text{ }\mu\text{M}$ final concentration. For low temperature measurements the samples, held in 1-cm pathlength plastic cuvette, were suspended, immediately before cooling, in a buffer containing 60% (w/v) glycerol as a cryoprotectant to obtain transparent matrixes. The plastic cuvette was placed in a flow cryostat (Oxford mod. Optistat CF) equipped with temperature control unit (ICT-503, Oxford Instruments).

Time-resolved fluorescence

Fluorescence decays were measured at 278 and 293 K by time-correlated single-photon counting using an instrument described earlier (Akhtar et al., 2020). Excitation pulses centered at 632 nm at 20 MHz repetition rate and ~ 0.1 -pJ energy, were obtained from a Fianium WhiteLase Micro (NKT Photonics, UK) supercontinuum laser. The PSII CC suspension was diluted to an absorbance of 0.03 at the excitation wavelength in reaction buffer supplemented with 20- μ M DCMU in a 3-mm pathlength flow cell. The sample was continuously circulated during the measurement to avoid repeated excitation of the same sample volume. Fluorescence decays were recorded at 685 nm and binned in 4 ps time channels. The total instrument response function (IRF) width was ~ 50 ps measured using 1% Ludox (colloidal silica) as scattering medium. The fluorescence lifetimes were determined by multiexponential fitting of the fluorescence decay kinetics combined with iterative re-convolution with the IRF using MATLAB routines created in-house.

To keep the RC open in the presence of DCMU, an open flow system was used, wherein the sample passed only once through the excitation beam at a flow rate of 200 μ L s^{-1} . Under these conditions, approximate F_o level was achieved. Baseline measurements were performed without DCMU and adding 25- μ M dichlophenolindophenol and 0.5-mM FeCy to make sure that RCs are fully open. For the approximate F_1 level, STSFs were applied (Excelitas LS-1130-3 Flashpac with FX-1163 Flashtube with reflector) at 2-Hz repetition rate corresponding to a single flash per sample passage. For measurements of light-adapted closed-state PSII (F_m level), the sample was pre-illuminated with a background light from a Schott KL 2500 LED lamp.

Supplemental data

The following materials are available in the online version of this article.

Supplemental Figure 1. Kinetic traces (A) and parameters (B) of STSF-induced Chl-*a* fluorescence yield transients of DCMU-treated dimeric and monomeric PSII CCs of *T. vulcanus* at 278 K.

Supplemental Figure 2. Amplitudes of the light-induced C550 absorbance transients of DCMU-treated PSII CC of *T. vulcanus* in the absence and presence of 2-mM dithionite.

Supplemental Figure 3. STSF-induced transient absorption spectra of DCMU-treated PSII CC of *T. vulcanus* in the presence and absence of 2-mM ferricyanide (FeCy) 2 ms after the excitation.

Supplemental Figure 4. Effects of dithionite and ferricyanide on the STSF-induced Chl-*a* fluorescence induction of DCMU-treated isolated spinach thylakoid membranes at 213 K.

Supplemental Figure 5. Chl-*a* fluorescence induction kinetics of DCMU-treated PSII CCs of *T. vulcanus* at 80 K (A) and at 173 and 233 K (B).

Supplemental Figure 6. Relaxation of F_m of F695 and F685 of DCMU-treated PSII CC of *T. vulcanus* at 80 K.

Supplemental Figure 7. Variations of the 80 K F_m fluorescence emission spectra of DCMU-treated PSII CC of *T. vulcanus* exposed to different preillumination protocols at 233 K.

Supplemental Figure 8. Comparison of F_o and F_m fluorescence emission spectra, normalized at 695 nm, of DCMU-treated PSII CC of *T. vulcanus* at different temperatures, as indicated.

Supplemental Figure 9. Decay-associated spectra of PSII CC of *T. vulcanus* obtained from four-exponential global analysis of fluorescence decays measured by TCSPC at 293 K.

Supplemental Figure 10. Kinetic model fitting of the fluorescence decays of PSII CC recorded by TCSPC at 278 K and emission wavelength 680 nm in F_1 and F_m conditions.

Supplemental Figure 11. Overall structure of PSII core complex from *T. vulcanus* (PDB: 5GTH) and schematic representation of the stationary (A) and transient (B) electric field, and the superposition (C) of the two fields due to the presence of Q_A^- and the $P680^+Pheo^-$ radical pair, respectively—characterized by equipotential profiles.

Supplemental Table 1. STSF-induced absorption changes of PSII CC of *T. vulcanus* and spinach thylakoid membranes in the presence of 40- μ M DCMU and 2-mM FeCy with and without waiting times ($\Delta\tau$) between flashes.

Supplemental Table 2. Effects of dithionite on the variations of the STSF-induced Chl-*a* fluorescence yields of DCMU-treated PSII CC of *T. vulcanus* at 278 K.

Acknowledgments

The authors are indebted to Profs. Govindjee, P. Joliot, A.W. Rutherford, T. Noguchi, and A.R. Holzwarth for helpful discussions. The authors also benefited from numerous stimulating discussions with Profs. A. Dér and L. Zimányi. We thank to Dr. W. Leibl for his help in configuring the FTIR experiments and for critical reading of the manuscript and to Dr. L. Kovács for recording the thermoluminescence glow curves on PSII CC.

Funding

The authors acknowledge the support from the Hungarian Ministry of Innovation and Technology, National Research, Development and Innovation Fund (OTKA grants KH-124985 and K-128679 to G.G.; PD-121225 to M.M.; and NN-124904 to P.H.L., who also used support from the grant 2018-1.2.1-NKP-2018-00009.) G.G. also acknowledges the support from TÉT 2018-2.1.14-TÉT-CN-2018-00004 from the Hungarian Ministry of Innovation and Technology, the Czech Science Foundation (GA ČR 19-13637S), and the Eötvös Loránd Research Network (ELKH KÜ-37/2020). M.M. and G.S. acknowledge the support from COST Actions CM1306 STSM Grant (ref. No.: 40047) and CA15126 STSM Grant (ref. No.: 41468), respectively. S.S. obtained support from the Grant Fondazione Cariplo (CYAO Project) Grant Number 2016-0667. J.-R.S., G.H., Q.Z., and Y.X. acknowledge the support from a National Key R&D Program of China

(2017YFA0503700), a Strategic Priority Research Program of the Chinese Academy of Sciences (XDB17000000) and a National Natural Science Foundation of China (31470339). P.A. used funds from a grant to ELI-ALPS project (GINOP-2.3.6-15-2015-00001), which is supported by the European Union and co-financed by the European Regional Development Fund. G.G. would like to dedicate this paper to the memory of his friend and colleague, Jacques Breton, whose hospitality in the lab and in his home are remembered with sentiments.

Conflict of interest statement. None declared.

References

- Abgaryan GA, Christophorov LN, Goushcha AO, Holzwarth AR, Kharkyanen VN, Knox PP, Lukashev EA** (1998) Effects of mutual influence of photoinduced electron transitions and slow structural rearrangements in bacterial photosynthetic reaction centers. *J Biol Phys* **24**: 1–17
- Akhtar P, Nowakowski PJ, Wang W, Do TN, Zhao S, Siligardi G, Garab G, Shen JR, Tan HS, Lambrev PH** (2020) Spectral tuning of light-harvesting complex II in the siphonous alga *Bryopsis corticulans* and its effect on energy transfer dynamics. *Biochim Biophys Acta Bioenerg* **1861**: 148191
- Andrizhiyevskaya EG, Chojnicka A, Bautista JA, Diner BA, van Grondelle R, Dekker JP** (2005) Origin of the F685 and F695 fluorescence in photosystem II. *Photosynth Res* **84**: 173–180
- Årsköld SP, Masters VM, Prince BJ, Smith PJ, Pace RJ, Krausz E** (2003) Optical spectra of synechocystis and spinach photosystem II preparations at 1.7 K: identification of the D1-pheophytin energies and stark shifts. *J Am Chem Soc* **125**: 13063–13074
- Barber J** (2004) Engine of life and big bang of evolution: a personal perspective. *Photosynth Res* **80**: 137
- Barber J, Melis A** (1990) Quantum efficiency for the photoaccumulation of reduced pheophytin in Photosystem II. *Biochim Biophys Acta* **1020**: 285–289
- Berthomieu C, Nabedryk E, Mantele W, Breton J** (1990) Characterization by FTIR spectroscopy of the photoreduction of the primary quinone acceptor QA in photosystem II. *FEBS Lett* **269**: 363–367
- Butler WL** (1978) Energy distribution in the photochemical apparatus of photosynthesis. *Annu Rev Plant Physiol* **29**: 345–378
- Butler WL, Okayama S** (1971) The photoreduction of C550 in chloroplasts and its inhibition by lipase. *Biochim Biophys Acta* **245**: 237–239
- Büchel C, Garab G** (1995) Electrochromic absorbency changes in the chlorophyll-*c*-containing alga *Pleurochloris-Meiringerensis* (Xanthophyceae). *Photosynth Res* **43**: 49–56
- Caffarri S, Broess K, Croce R, van Amerongen H** (2011) Excitation energy transfer and trapping in higher plant Photosystem II complexes with different antenna sizes. *Biophys J* **100**: 2094–2103
- Cardona T, Sedoud A, Cox N, Rutherford AW** (2012) Charge separation in photosystem II: a comparative and evolutionary overview. *Biochim Biophys Acta Bioenerg* **1817**: 26–43
- Ceppi MG, Oukarroum A, Cicek N, Strasser RJ, Schansker G** (2012) The IP amplitude of the fluorescence rise OJIP is sensitive to changes in the photosystem I content of leaves: a study on plants exposed to magnesium and sulfate deficiencies, drought stress and salt stress. *Physiol Plant* **144**: 277–288
- Chmeliov J, Trinkunas G, van Amerongen H, Valkunas L** (2014) Light harvesting in a fluctuating antenna. *J Am Chem Soc* **136**: 8963–8972
- Chylla RA, Garab G, Whitmarsh J** (1987) Evidence for slow turnover in a fraction of photosystem II complexes in thylakoid membranes. *Biochim Biophys Acta* **894**: 562–571
- Connolly JS, Samuel EB, Janzen AF** (1982) Effects of solvent on the fluorescence properties of bacteriochlorophyll *a*. *Photochem Photobiol* **36**: 565–574
- Cseh Z, Rajagopal S, Tsonev T, Busheva M, Papp E, Garab G** (2000) Thermo-optic effect in chloroplast thylakoid membranes. Thermal and light stability of pigment arrays with different levels of structural complexity. *Biochemistry* **39**: 15250–15257
- Dau H, Sauer K** (1992) Electric-field effect on the picosecond fluorescence of Photosystem-II and its relation to the energetics and kinetics of primary charge separation. *Biochim Biophys Acta* **1102**: 91–106
- Delosme R** (1967) Study of the induction of fluorescence in green algae and chloroplasts at the onset of an intense illumination. *Biochim Biophys Acta* **143**: 108–128
- Demmig-Adams B, Stewart JJ, Burch TA, Adams WW, 3rd** (2014) Insights from placing photosynthetic light harvesting into context. *J Phys Chem Lett* **5**: 2880–2889
- Duysens LMN, Sweers HE** (1963) Studies on Microalgae and Photosynthetic Bacteria. Japanese Society of Plant Physiologists, University of Tokyo Press, Tokyo
- Duysens LN** (1978) Transfer and trapping of excitation energy in photosystem II. *Ciba Found Symp* **61**: 323–340
- Farooq S, Chmeliov J, Wientjes E, Koehorst R, Bader A, Valkunas L, Trinkunas G, van Amerongen H** (2018) Dynamic feedback of the photosystem II reaction centre on photoprotection in plants. *Nat Plants* **4**: 225–231
- Feyziyev Y, Deák Z, Styring S, Bernát G** (2013) Electron transfer from Cyt b559 and tyrosine-D to the S2 and S3 states of the water oxidizing complex in photosystem II at cryogenic temperatures. *J Bioenerg Biomembr* **45**: 111–120
- France LL, Geacintov NE, Breton J, Valkunas L** (1992) The dependence of the degrees of sigmoidicity of fluorescence induction curves in spinach-chloroplasts on the duration of actinic pulses in pump-probe experiments. *Biochim Biophys Acta* **1101**: 105–119
- Fried SD, Boxer SG** (2017) Electric fields and enzyme catalysis. *Annu Rev Biochem* **86**: 387–415
- Genty B, Briantais JM, Baker NR** (1989) The relationship between the quantum yield of photosynthetic electron-transport and quenching of chlorophyll fluorescence. *Biochim Biophys Acta* **990**: 87–92
- Hodges M, Moya I** (1986) Time-resolved chlorophyll fluorescence studies of photosynthetic membranes - resolution and characterization of 4 kinetic components. *Biochim Biophys Acta* **849**: 193–202
- Holzwarth AR, Wendler J, Haehnel W** (1985) Time-resolved picosecond fluorescence-spectra of the antenna chlorophylls in *Chlorella-vulgaris* - resolution of Photosystem-I fluorescence. *Biochim Biophys Acta* **807**: 155–167
- Hou JM, Boichenko VA, Diner BA, Mauzerall D** (2001) Thermodynamics of electron transfer in oxygenic photosynthetic reaction centers: volume change, enthalpy, and entropy of electron-transfer reactions in manganese-depleted photosystem II core complexes. *Biochemistry* **40**: 7117–7125
- Ikegami I, Katoh S** (1973) Studies on chlorophyll fluorescence in chloroplasts II. Effect of ferricyanide on the induction of fluorescence in the presence of 3-(3,4-dichlorophenyl)-1,1-dimethylurea. *Plant Cell Physiol* **14**: 829–836
- Joliot A, Joliot P** (1964) Étude cinétique de la réaction photochimique libérant l'oxygène au cours de la photosynthèse. *CR Acad Sci Paris* **258**: 4622–4625
- Joliot P, Joliot A** (1979) Comparative study of the fluorescence yield and of the C550 absorption change at room temperature. *Biochim Biophys Acta* **546**: 93–105
- Kálmán L, Maróti P** (1997) Conformation-activated protonation in reaction centers of the photosynthetic bacterium *Rhodospira sphaeroides*. *Biochemistry* **36**: 15269–15276
- Kawakami K, Shen JR** (2018) Purification of fully active and crystallizable photosystem II from thermophilic cyanobacteria. *Methods Enzymol* **613**: 1–16

- Kern J, Alonso-Mori R, Tran R, Hattne J, Gildea RJ, Echols N, Glockner C, Hellmich J, Laksmono H, Sierra RG, et al.** (2013) Simultaneous femtosecond X-ray spectroscopy and diffraction of Photosystem II at room temperature. *Science* **340**: 491–495
- Kleinfeld D, Okamura MY, Feher G** (1984) Electron-transfer kinetics in photosynthetic reaction centers cooled to cryogenic temperatures in the charge-separated state: evidence for light-induced structural changes. *Biochemistry* **23**: 5780–5786
- Klimov VV, Klevanik AV, Shuvalov VA, Kransnovsky AA** (1977) Reduction of pheophytin in the primary light reaction of photosystem II. *FEBS Lett* **82**: 183–186
- Knox PP, Venediktov PS, Kononenko AA, Garab GI, Faludidaniel A** (1984) Role of electric polarization in the thermo-luminescence of chloroplasts. *Photochem Photobiol* **40**: 119–125
- Koike H, Inoue Y** (1983) Preparation of oxygen-evolving photosystem II particles from a thermophilic blue-green alga. In Y Inoue, AR Crofts, Govindjee, N Murata, G Renger, K Satoh, eds, *The Oxygen Evolving System of Photosynthesis*. San Diego, CA: Academic Press, pp 257–263
- Kupitz C, Basu S, Grotjohann I, Fromme R, Zatsepin NA, Rendek KN, Hunter MS, Shoeman RL, White TA, Wang D, et al.** (2014) Serial time-resolved crystallography of photosystem II using a femtosecond X-ray laser. *Nature* **513**: 261–265
- Laisk A, Oja V** (2020) Variable fluorescence of closed photochemical reaction centers. *Photosynth Res* **143**: 335–346
- Lavergne J, Trissl HW** (1995) Theory of fluorescence induction in Photosystem-II - derivation of analytical expressions in a model including exciton-radical-pair equilibrium and restricted energy-transfer between photosynthetic units. *Biophys J* **68**: 2474–2492
- Magyar M, Sipka G, Kovács L, Ughy B, Zhu Q, Han G, Špunda V, Lambrev PH, Shen JR, Garab G** (2018) Rate-limiting steps in the dark-to-light transition of Photosystem II - revealed by chlorophyll-*a* fluorescence induction. *Sci Rep* **8**: 2755
- Malferrari M, Mezzetti A, Francia F, Venturoli G** (2013) Effects of dehydration on light-induced conformational changes in bacterial photosynthetic reaction centers probed by optical and differential FTIR spectroscopy. *Biochim Biophys Acta Bioenerg* **1827**: 328–339
- Mezzetti A, Leibl W** (2017) Time-resolved infrared spectroscopy in the study of photosynthetic systems. *Photosynth Res* **131**: 121–144
- Mezzetti A, Nabedryk E, Breton J, Okamura MY, Paddock ML, Giacometti G, Leibl W** (2002) Rapid-scan Fourier transform infrared spectroscopy shows coupling of Glu-L212 protonation and electron transfer to QB in *Rhodobacter sphaeroides* reaction centers. *Biochim Biophys Acta* **1553**: 320–330
- Nabedryk E, Bagley KA, Thibodeau DL, Bauscher M, Mäntele W, Breton J** (1990) A protein conformational change associated with the photoreduction of the primary and secondary quinones in the bacterial reaction center. *FEBS Lett* **266**: 59–62
- Nagy L, Maróti P, Terazima M** (2008) Spectrally silent light induced conformation change in photosynthetic reaction centers. *FEBS Lett* **582**: 3657–3662
- Nakanishi M, Sokolov AP** (2015) Dielectric spectroscopy of hydrated biomacromolecules. In V Raicu, Y Feldman, eds, *Dielectric Relaxation in Biological Systems*. Oxford University Press, Oxford
- Nelson N, Yocum CF** (2006) Structure and function of photosystems I and II. *Annu Rev Plant Biol* **57**: 521–565
- Nematov S, Casazza AP, Remelli W, Khuvondikov V, Santabarbara S** (2017) Spectral dependence of irreversible light-induced fluorescence quenching: chlorophyll forms with maximal emission at 700-702 and 705-710nm as spectroscopic markers of conformational changes in the core complex. *Biochim Biophys Acta Bioenerg* **1858**: 529–543
- Noguchi T** (2007) Light-induced FTIR difference spectroscopy as a powerful tool toward understanding the molecular mechanism of photosynthetic oxygen evolution. *Photosynth Res* **91**: 59–69
- Onoda K, Mino H, Inoue Y, Noguchi T** (2000) An FTIR study on the structure of the oxygen-evolving Mn-cluster of Photosystem II in different spin forms of the S₂ state. *Photosynth Res* **63**: 47–57
- Papageorgiou GC, Govindjee** (2004) *Chlorophyll a Fluorescence: A Signature of Photosynthesis*. Springer, Dordrecht, The Netherlands
- Remelli W, Santabarbara S** (2018) Excitation and emission wavelength dependence of fluorescence spectra in whole cells of the cyanobacterium *Synechocystis sp.* PPC6803: influence on the estimation of Photosystem II maximal quantum efficiency. *Biochim Biophys Acta Bioenerg* **1859**: 1207–1222
- Rizzo F, Zucchelli G, Jennings R, Santabarbara S** (2014) Wavelength dependence of the fluorescence emission under conditions of open and closed Photosystem II reaction centres in the green alga *Chlorella sorokiniana*. *Biochim Biophys Acta Bioenerg* **1837**: 726–733
- Roelofs TA, Lee CH, Holzwarth AR** (1992) Global target analysis of picosecond chlorophyll fluorescence kinetics from pea-chloroplasts - a new approach to the characterization of the primary processes in Photosystem-II alpha-units and beta-units. *Biophys J* **61**: 1147–1163
- Romero E, Novoderezhkin VI, van Grondelle R** (2017) Quantum design of photosynthesis for bio-inspired solar-energy conversion. *Nature* **543**: 355–365
- Ruban AV** (2016) Nonphotochemical chlorophyll fluorescence quenching: mechanism and effectiveness in protecting plants from photodamage. *Plant Physiol* **170**: 1903–1916
- Schansker G, Toth SZ, Strasser RJ** (2005) Methylviologen and dibromothymoquinone treatments of pea leaves reveal the role of photosystem I in the Chl *a* fluorescence rise OJIP. *Biochim Biophys Acta* **1706**: 250–261
- Schansker G, Tóth SZ, Holzwarth AR, Garab G** (2014) Chlorophyll *a* fluorescence: beyond the limits of the Q_A model. *Photosynth Res* **120**: 43–58
- Schansker G, Tóth SZ, Kovács L, Holzwarth AR, Garab G** (2011) Evidence for a fluorescence yield change driven by a light-induced conformational change within photosystem II during the fast chlorophyll *a* fluorescence rise. *Biochim Biophys Acta Bioenerg* **1807**: 1032–1043
- Shen J-R** (1998) Possible functional differences between dimer and monomer of Photosystem II complex. In G Garab, ed, *Photosynthesis: Mechanisms and Effects: Volume I–V: Proceedings of the XIth International Congress on Photosynthesis*, Budapest, Hungary, 17–22 August 1998, pp. 941–944
- Shen JR, Inoue Y** (1993) Binding and functional-properties of two new extrinsic components, cytochrome *c*-550 and a 12-kDa Protein, in cyanobacterial photosystem II. *Biochemistry* **32**: 1825–1832
- Shen JR, Kamiya N** (2000) Crystallization and the crystal properties of the oxygen-evolving photosystem II from *Synechococcus vulcanus*. *Biochemistry* **39**: 14739–14744
- Shen JR, Kawakami K, Koike H** (2011) Purification and crystallization of oxygen-evolving photosystem II core complex from thermophilic cyanobacteria. *Methods Mol Biol* **684**: 41–51
- Shibata Y, Nishi S, Kawakami K, Shen JR, Renger T** (2013) Photosystem II does not possess a simple excitation energy funnel: time-resolved fluorescence spectroscopy meets theory. *J Am Chem Soc* **135**: 6903–6914
- Shlyk-Kerner O, Samish I, Kaftan D, Holland N, Sai PSM, Kless H, Scherz A** (2006) Protein flexibility acclimatizes photosynthetic energy conversion to the ambient temperature. *Nature* **442**: 827–830
- Sipka G, Kis M, Maróti P** (2018) Characterization of mercury(II)-induced inhibition of photochemistry in the reaction center of photosynthetic bacteria. *Photosynth Res* **136**: 379–392
- Sipka G, Müller P, Brettel K, Magyar M, Kovács L, Zhu QJ, Xiao YA, Han GY, Lambrev PH, Shen JR, et al.** (2019) Redox transients of P680 associated with the incremental chlorophyll-*a* fluorescence yield rises elicited by a series of saturating flashes in diuron-treated photosystem II core complex of *Thermosynechococcus vulcanus*. *Physiol Plant* **166**: 22–32
- Stirbet A** (2013) Excitonic connectivity between photosystem II units: what is it, and how to measure it? *Photosynth Res* **116**: 189–214

- Stirbet A, Govindjee** (2012) Chlorophyll a fluorescence induction: a personal perspective of the thermal phase, the J-I-P rise. *Photosynth Res* **113**: 15–61
- Strasser RJ, Tsimilli-Michael M, Srivastava A** (2004) Analysis of the chlorophyll a fluorescence transient. *In* GC Papageorgiou, Govindjee, eds, *Chlorophyll a Fluorescence: A Signature of Photosynthesis*. Springer, Dordrecht, The Netherlands, pp 463–495
- Suga M, Akita F, Sugahara M, Kubo M, Nakajima Y, Nakane T, Yamashita K, Umena Y, Nakabayashi M, Yamane T, et al.** (2017) Light-induced structural changes and the site of O=O bond formation in PSII caught by XFEL. *Nature* **543**: 131–135
- Szczepaniak M, Sander J, Nowaczyk M, Müller MG, Rögner M, Holzwarth AR** (2009) Charge separation, stabilization, and protein relaxation in photosystem II core particles with closed reaction center. *Biophys J* **96**: 621–631
- Tracewell CA, Brudvig GW** (2008) Multiple redox-active chlorophylls in the secondary electron-transfer pathways of oxygen-evolving Photosystem II. *Biochemistry* **47**: 11559–11572
- Treves H, Raanan H, Kedem I, Murik O, Keren N, Zer H, Berkowicz SM, Giordano M, Norici A, Shotland Y, et al.** (2016) The mechanisms whereby the green alga *Chlorella ohadii*, isolated from desert soil crust, exhibits unparalleled photodamage resistance. *New Phytol* **210**: 1229–1243
- Tyystjarvi E, Vass I** (2004) Light emission as a probe of charge separation and recombination in the photosynthetic apparatus: relation of prompt fluorescence to delayed light emission and thermoluminescence. *In* GC Papageorgiou, Govindjee, eds, *Chlorophyll a Fluorescence. Advances in Photosynthesis and Respiration*. Springer, Dordrecht, The Netherlands, pp 363–388
- van Amerongen H, Croce R** (2013) Light harvesting in Photosystem II. *Photosynth Res* **116**: 251–263
- van der Weij-de Wit CD, Dekker JP, van Grondelle R, van Stokkum IHM** (2011) Charge separation is virtually irreversible in Photosystem II core complexes with oxidized primary quinone acceptor. *J Phys Chem A* **115**: 3947–3956
- Vavilin DV, Ermakova-Gerdes SY, Keilty AT, Vermaas WF** (1999) Tryptophan at position 181 of the D2 protein of photosystem II confers quenching of variable fluorescence of chlorophyll: implications for the mechanism of energy-dependent quenching. *Biochemistry* **38**: 14690–14696
- Vredenberg W** (2011) Kinetic analyses and mathematical modeling of primary photochemical and photoelectrochemical processes in plant photosystems. *Biosystems* **103**: 138–151
- Witt HT** (1979) Energy-conversion in the functional membrane of photosynthesis - analysis by light-pulse and electric pulse methods - central role of the electric-field. *Biochim Biophys Acta* **505**: 355–427
- Zimányi L, Garab G** (1989) Configuration of the electric-field and distribution of ions in energy transducing biological membranes: model calculations in a vesicle containing discrete charges. *J Theor Biol* **138**: 59–76